6th International Conference on Multiphase Flow,
ICMF 2007, Leipzig, Germany, July 9–13, 2007

Study of hydrodynamic characteristics of the liquid layer during counter-current flow in inclined small diameter tubes: the effect of liquid properties

Maria N. Pantzali, Aikaterini A. Mouza, Spiros V. Paras

Aristotle University of Thessaloniki, Department of Chemical Engineering
Laboratory of Chemical Process and Plant Design
Univ. Box 455, Thessaloniki, GR 54124, Greece
mouza@cheng.auth.gr

Keywords: flooding, liquid layer, inclination, small diameter tube, liquid properties

Abstract

This is an experimental investigation on the effect of inclination angle and liquid properties on flooding phenomena and liquid layer characteristics in small diameter tubes (i.e., 7 and 9 mm). Experiments have been carried out at various inclination angles from the horizontal (30°, 45° and 60°), while several liquids are employed covering a wide range of physical properties. Fast video recordings and the conductivity method are used for liquid layer thickness characteristics measurement and statistical analysis, while the wall shear stress at the tube bottom centerline is measured using the electrodiffusion technique. At low liquid flow rates flooding is initiated due to lateral liquid spreading facilitated by the large tube curvature At higher liquid flow rates the growth and reversal of 3-D waves is the mechanism for incipient flooding. At even higher liquid flow rates the growth of disturbances at liquid inlet is the cause of flooding.

Introduction

The operation and performance of many industrial devices, such as compact reflux condensers, desiccant cooling systems etc are limited by the phenomenon of flooding. Flooding is initiated during gas-liquid counter-current flow, when at least part of the liquid flow is reversed in direction and carried by the gas above its injection point. The study of flooding in inclined small diameter tubes is expected to contribute towards improved design and operation of equipment, where the flow passages are characterized by equivalent diameters less than 10 mm.

Extensive research work has been carried out over the past few decades concerning flooding. Bankoff & Lee (1986) and Hewitt (1995) have published critical reviews on the work done in this area. However, there is still considerable uncertainty related to the prevailing mechanisms and a lack of reliable predictive tools of general validity. The most important factors that tend to influence the onset of flooding are the conduit geometry, the type of liquid and gas entry and the properties of the liquid phase. The most common correlation, though often unsuccessful, is that of Wallis (1969) that takes into account the conduit geometry as well as the superficial velocities and the densities of the two phases. Efforts have been made to improve this correlation, by including more parameters that affect the phenomenon, such as all liquid properties and the tube inclination angle (e.g. Zapke & Kroeger, 1996, 2000a, 2000b).

The majority of the relative studies are based on experiments in *large* diameter *vertical* tubes. The general trend observed is an increased flooding velocity with increasing tube i.d. (e.g. Koizumi & Ueda, 1996; Mouza et al., 2002). However, according to the literature (e.g. Jayanti et al., 1996; Mouza et al., 2002), the tube diameter also affects the flooding mechanism; the gas velocity needed to transport a wave upwards increases with the tube diameter and therefore for large diameter tubes the "*entrainment and carryover of droplets*" mechanism prevails, while for smaller i.d. tubes "*wave transport*" is encountered.

The work available in the literature concerning **inclined** tubes is quite limited and the majority refers to large diameter tubes, i.e., D≥20 mm (e.g. Barnea et al., 1986; Celata et al., 1992; Zapke & Kroeger, 1996, Wongwises, 1998). The work of Barnea et al. (1986) covers the widest range of inclination angles (1–90° from horizontal) for air–water counter-current flow in a 51 mm i.d. tube. According to their observations, as inclination increases, the gas-liquid interfacial area increases due to the distribution of the liquid layer around the periphery and the flow rates at which flooding occurs increase and then decrease as the vertical position is approached. A similar observation is made by Fiedler et al. (2002), who studied reflux condensation in an inclined 7 mm i.d. tube using the refrigerant R134a, and found that the highest flooding velocity occurs for inclination between 45° and 60° from the horizontal. Maximum flooding velocities at 45° for the lower liquid flow rates were also observed by Ousaka et al. (2006), who studied flooding in a 16 mm diameter inclined tube. They also suggest that this maximum shifts to higher angles for higher liquid flow rates.

The literature review reveals that the effect of liquid physical properties on flooding has not been completely clarified. For example, it has been reported that in vertical tubes the critical flooding velocity tends to decrease with increasing liquid viscosity (e.g. Clift et al., 1966; Mouza et al., 2005). However, Suzuki & Ueda (1977), who conducted experiments in 10, 18 and 28.8 mm i.d. vertical tubes, reported an increase of flooding velocity with increasing liquid viscosity. High

viscosity liquids exhibit thick free falling liquid layers and large amplitude waves grow even for very low Reynolds numbers and tend to increase with liquid flow rate, a fact that facilitates flooding (e.g. Mouza et al., 2005; Nguyen & Balakotaiah, 2000). Suzuki & Ueda (1977) studied the effect of surface tension and they reported that flooding velocity takes its maximum value at a condition where the surface tension is close to 50 mN/m. Ousaka et al. (2006) concluded that flooding velocity decreases with surface tension, while Mouza et al. (2005) found that surface tension results to more wavy interface. English et al. (1963) report that surfactant solutions seem to be more wetting and spread around the tube walls. According to Zapke & Kroeger (1996, 2000a) the role of liquid viscosity and surface tension is secondary to that of the phase densities. The liquid viscosity was found to have a stronger effect, while surface tension has a very small stabilizing effect. Their effect on flooding is smaller in the inclined than in the vertical case.

Theoretical approaches of the flooding phenomenon have been also attempted, recognizing that it is caused by the complicated interaction of gas flow with a wavy liquid layer interface (e.g. Cetinbudaklar & Jameson, 1969; Shearer & Davidson, 1965). The success of such efforts that are based on liquid wave growth and stability analysis has been limited at best.

An important factor affecting incipient flooding is the structure and characteristics of the gas-liquid interface ***prior*** to flooding. According to several researchers (e.g. Dukler et al., 1984; Zabaras & Dukler, 1988) the mean liquid layer thickness remains essentially unaffected by the counter-current gas flow almost up to the critical flooding conditions. It is therefore considered advantageous to use relevant information on wavy free falling liquid layers to clarify the onset of flooding. However, systematically obtained falling liquid layer data for flow inside *small* diameter inclined tubes are not available in the literature, to the authors' best knowledge. Limited data concerning free falling kerosene layers in small diameter inclined tubes have been published by Mouza et al. (2003).

In experiments conducted in this Laboratory incipient flooding in *vertical* (Mouza et al., 2002, 2005) and inclined (Mouza et al., 2003) *small* diameter tubes has been studied, showing that the flooding curve shape and mechanism differ considerably between vertical and inclined tubes (***Figure 1***).

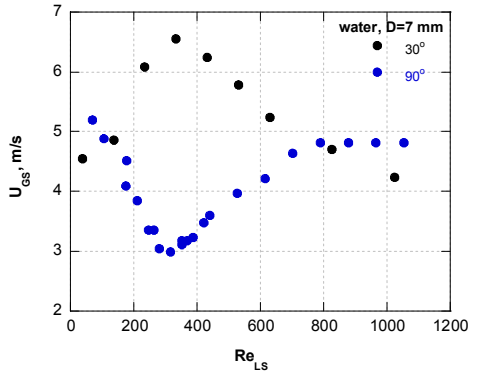

Figure 1: Typical flooding curves for water in inclined and vertical tubes (Mouza et al., 2002, 2003).

They also suggest that the large tube curvature affects liquid layer flow development, possibly promoting wave interaction and damping. Finally, it is interesting that the critical flooding velocities in vertical tubes are significantly lower than those corresponding to inclined tubes, all other conditions being the same. In turn, the wavy liquid layer evolution essentially determines flooding characteristics and in all cases studied the dominant mechanism is wave growth and upward dragging by the gas. It has been observed that the flooding curves exhibit a trend different than the one usually reported in the literature. More specifically, in the case of inclined tubes, and for lower liquid flow rates flooding velocities increase with liquid Reynolds number, which can be attributed to the lateral spreading of the liquid facilitated by the large tube curvature (i.e., small tube i.d.). As liquid flow rate increases this trend is reversed and the flooding velocity decreases with increasing liquid flow rate. In this region the mechanism for incipient flooding is the growth of 3-D waves and reversal of their flow direction. Finally, at relatively high flow rates the flooding velocity tends to reach a constant value that is attributed to the growth of disturbances at liquid inlet and flow reversal at this point (Mouza et al., 2003). Flooding curves, however, differ depending on many factors, such as the liquid properties, the tube diameter and the inclination angle. The effect of the liquid properties has been studied extensively for the vertical case and correlations have been proposed for the prediction of the flooding velocities (Mouza et al., 2005).

The present work is focused on the influence of inclination angle and liquid properties on the liquid layer characteristics and flooding mechanisms. After a brief description of experimental equipment and procedures the critical flooding velocities and related observations are presented. Experimental data on hydrodynamic characteristics of the liquid layers are reported next, in an attempt to elucidate the two-phase flow behaviour.

Nomenclature

C_0	concentration of the active ions (kmol/m^3)
D	tube diameter (m)
D_i	diffusion coefficient (m^2/s)
F	Faraday constant (9.648x10^{7}C/kmol)
H	total thickness measured with the optical method (m)
h	liquid layer thickness (m)
I	total probe current (A)
l	distance from the probe front edge (m)
Q	volumetric flow rate (l/min)
t	time (s)
t_w	tube wall thickness (m)
U	velocity (m/s)
w	width of the probe strip (m)
z	number of electrons involved in the redox reaction

Greek letters

γ	shear rate (s^{-1})
μ	dynamic viscosity (kg/ms)
σ	surface tension (kg/s^2)
τ_w	wall shear stress (kg/ms^2)
φ	tube inclination angle

Subsripts

ave	average
b	at the bottom centerline
G	gas
L	liquid
rms	root mean square value
S	superficial

Experimental Setup and Procedures

The flooding and falling liquid layer experiments are carried out in transparent cylindrical tubes (made of glass or *Plexiglas®)* with small i.d. (7 and 9 mm) and a length of 0.6 m. The experimental setup is shown in ***Figure 2a***. The liquid flows down the tube, while the gas phase is in counter-current flow. To ensure smooth inlet and outlet conditions, so as to minimize disturbances, specially machined Plexiglas® sections are used. The liquid is introduced from the top of the tube by overflow (***Figure 2b)***, while compressed air, used as the gas phase, enters through a small tube at the bottom placed concentrically to the main tube. The liquid phase comes out at the bottom through a conical section, so as to minimize end-effects, and is collected in a small tank, whose level is kept constant, higher than the point where the liquid is discharged, to ensure there is no air leakage (***Figure 2c***). This system can be fixed at different angles (i.e., 30°, 45° and 60° from the horizontal) so that the effect of the tube inclination can be studied. The liquid phase is stored in a 2-liter glass container and is recirculated by means of a centrifugal pump. The two-phase mixture coming out of the upper part of the tube during flooding is separated in a phase separator; air is released in the atmosphere whereas the liquid is driven back in the tank. The flow of the two phases is controlled with manual valves.

In order to study the influence of liquid properties on flooding phenomena several liquids have been used (i.e., water, and aqueous glycerine, butanol and Tween®80 solutions) covering a sufficiently broad range of viscosity (1.0-19.5 mPa·s) and surface tension (35-72 mN/m) values. Tween®80 is an non-ionic surfactant. The liquids adopted and their physical properties, as experimentally measured, are listed in ***Table 1***.

Table 1: Physical properties of liquids employed (aqueous solution concentrations are expressed in %v/v).

Liquid	**index**	**ρ** kg/m^3	**μ** mPa·s	**σ** mN/m
water	w	998	1.0	72
aq. butanol 2%	but-2	995	0.9	47
aq. butanol 5%	but-5	998	0.9	35
aq. Tween®80 0.15%	tw	988	1.1	48
aq. glycerin 30%	gl-30	1080	2.3	69
aq. glycerin 50%	gl-50	1134	7.1	70
aq. glycerin 66%	gl-66	1180	19.6	66
aq. ferro-ferricyanide	fer	998	1.0	72

Direct visual observations were conducted using a Redlake MotionScope PCI® high-speed camera in order to study the falling liquid layer structure and to better understand the flooding mechanisms. The camera was fixed on a stand very close to the area of observation in such a way that the test section was located between the camera and the lighting system. The latter was comprised of several halogen lamps placed behind a diffuser to evenly distribute the light. The imaging system used was capable of recording up to 1000 full frames per second, but in the present experiments pictures were taken at a speed of 500 frames per second and a shutter rate of 1/2000 at a point near the liquid exit and a maximum recording time of 8 seconds, a constrain imposed by the camera software.

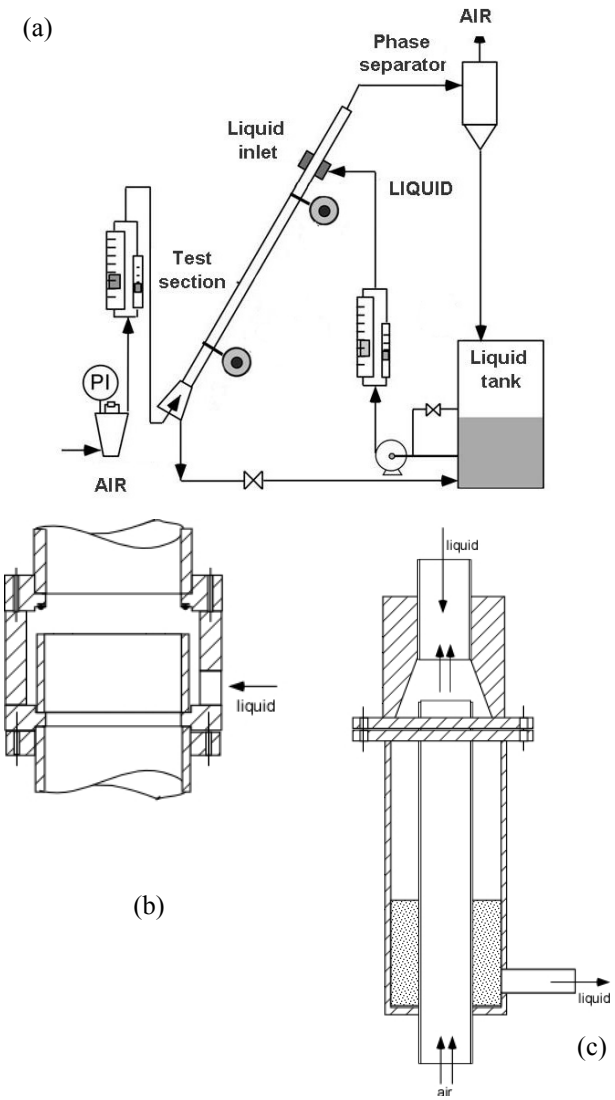

Figure 2: a) Experimental setup b) Liquid inlet section c) Liquid outlet- Gas inlet section.

The recorded images are used to extract *quantitative* information on the temporal variation of falling liquid layer thickness. With proper lighting the cross section of the tube along the tube axis and the liquid layer are clearly outlined on the pictures as shown in ***Figure 3a***, where the inside (*i.d.*) and the outside (*o.d.*) tube diameters as well as the tube wall thickness (t_w) and the measured "total thickness" (H) are depicted. The actual liquid layer thickness is obtained by subtracting the known wall thickness, t_w, from H. Using appropriate software (custom-made routines in MATLAB®) the layer trace can be obtained at a certain point along the tube. Calibration of the method is based on the diameter of a needle which is placed next to the wall of the tube (***Figure 3b***), where the fluid flows. The needle diameter is comparable with the liquid layer thickness values, i.e., 0.325 mm. As it can be seen in ***Figure 3b*** only two interfaces are visible, namely the air-liquid interface, which is changing as the fluid flows, and the outside edge of the tube. The liquid layer thickness is calculated by subtracting the known tube wall thickness from the measured thickness.

The software used for processing the recorded images, correlates the number of pixels between two points on the picture to a known length (e.g. the needle diameter). Accordingly any distance on the picture (e.g. Npixels) can be

converted in length units, based on the following relationship:

$$x = Mpixels\frac{d}{Npixels}$$

where *Mpixels* is the amount of pixels between two points, whose distance, d, is defined.

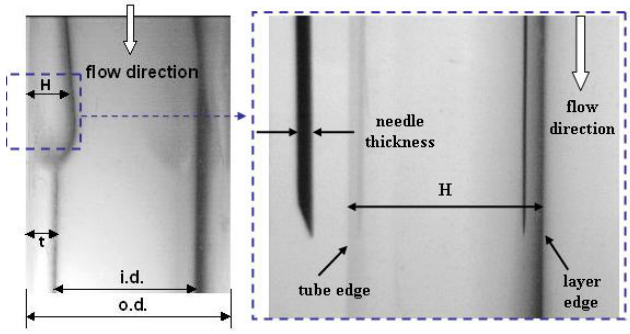

(a) (b)

Figure 3: a) Photo of the flow in the tube, b) detail of the liquid layer.

It must be noted that due to the cylindrical walls a certain distortion is inevitable. The uncertainty related to this distortion has been experimentally estimated to be less than 3% by measuring the static layer thickness in a horizontal tube section filled with known liquid quantities and for all liquids employed. However, the major measuring error seems to arise from the fact that the width of the line marking the gas-liquid interface (***Figure 3***) introduces an uncertainty with an absolute value in the order of 50 μm. This type of error depends only on the lighting and focusing conditions and it is independent of the measured liquid layer thickness. Thus, it is estimated that the uncertainty of this non-intrusive method is less than 10%, i.e., comparable with other widely used intrusive methods.

To overcome the recording time limitation of 8 seconds imposed by the video camera, the *parallel wire conductance technique* is also employed for obtaining longer layer thickness time-series, necessary for statistical and spectral analysis. This method is based on the proportionality of the electrical conductivity of the liquid layer and its thickness and is described in detail elsewhere (e.g. Paras & Karabelas, 1991). The probe adopted consists of two parallel stainless steel wires with a diameter of 0.33 mm. They are fixed in a removable part of the tube near the liquid exit and lie on a plane perpendicular to the liquid flow 0.5 mm apart from each other. However, in the case of so closely placed wires, a fact dictated by the large tube curvature, the liquid meniscus formed between the wires due to capillary forces, introduces a significant offset in the results. Consequently, even though this method is not suitable for extracting quantitative information of the liquid layer thickness, it can provide reliable information on its fluctuations. Moreover, this technique can not be used for counter-current flow because the wires may influence the onset of flooding.

The *electrodiffusion method* is adopted for shear stress measurements near the wall and the detection of the flow direction (Alekseenko et al., 1994; Mitchell & Hanratty, 1966). This non-intrusive method is based on a fast electrochemical reaction, whose rate is controlled by the diffusion of an ion near the tube wall. The diffusion rate is defined by measuring the current generated by the ion movement from the liquid mass to the cathode electrode and is correlated to the wall shear rate. The anode has a quite bigger surface area than the cathode, so that the total reaction rate is determined by the cathode. The reactions taking place on the cathode and the anode respectively are:

$$Fe(CN)_6^{3-} + e \rightarrow Fe(CN)_6^{4-}$$

$$Fe(CN)_6^{4-} \rightarrow Fe(CN)_6^{3-} + e$$

The probe applied is a two-segment probe (Tihon et al., 2003) that consists of two active platinum segment-strips (0.1x1 mm) separated by a thin insulating gap, embedded in a stainless steel tube with a 4 mm outside diameter (***Figure 4***). Each of the strips serves as a cathode, while the outer tube constitutes the anode. The probe is placed on the tube bottom centerline near the liquid exit, flush to the tube wall with the strips perpendicular to the liquid flow. The direction of the flow is detected by comparing the magnitudes of the current signals obtained from the front and rear probe segment. For a single strip-segment the current-signal can be related to the instantaneous value of wall shear rate using the formula:

$$I(t) = 0.807 z F c_0 w l^{2/3} D_i^{2/3} \gamma^{1/3}$$

The fluid used for the experiments is tap water containing equimolar 0.025 M potassium ferro- and ferricyanide and 0.057 M potassium sulfate as a supporting electrolyte that does not participate in the reaction but it is necessary in order to suppress migration current.

It is known that the wall shear stress variations are related to the liquid layer thickness fluctuations (Zabaras & Dukler, 1988). Therefore this non-intrusive method can be considered reliable for gaining insight into the interfacial shape during counter-current liquid-gas flow, where the optical and conductivity methods can not be adopted.

Data sets of shear stress and liquid layer thickness using the electrodiffusion and the conductivity method respectively are collected for a period up to ~40s with a sampling frequency of 0.5 kHz.

All the experiments involving visual observations were conducted using glass tubes (i.e., flooding curves, video camera method), while where the conductivity and the electrodiffusion methods were employed, Plexiglas® tubes were used to permit the use of the relevant probes.

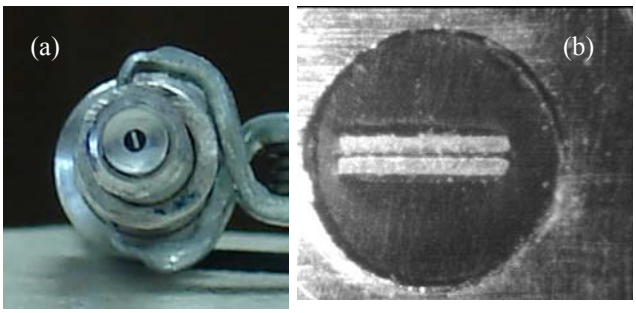

Figure 4: a) Shear stress probe, b) detail of the two strips

Results and Discussion

Flooding velocities

In this study the onset of flooding is visually defined, as the point where reversal of the liquid flow is initiated. A typical experimental flooding curve is presented in ***Figure 5***. The data are plotted in terms of superficial gas velocity, U_{GS}, and liquid flow rate, Q_L, at incipient flooding, where $U_{GS}=4Q_G/\pi D^2$. Three distinct regions are readily observed on the flooding curve. More specifically, for low liquid flow

rates the gas flooding velocity increases almost linearly with liquid flow rate (***Region A***), a trend that has also been observed by Mouza et al. (2003), who conducted experiments in a similar apparatus, using same diameter tubes. The extent of this region depends on the tube and its existence can be attributed to the tube curvature. This is the reason that it is not reported in the literature for experiments with larger diameter tubes.

After a critical liquid flow rate this trend is reversed (***Region B***) and the flooding velocity becomes inversely proportional to liquid flow rate, which is the common tendency encountered in flooding literature.

For even higher liquid velocities the liquid volume entering the tube tends to block the cross section at the inlet and thus flooding can be initiated even at very low gas flow rates (***Region C***).

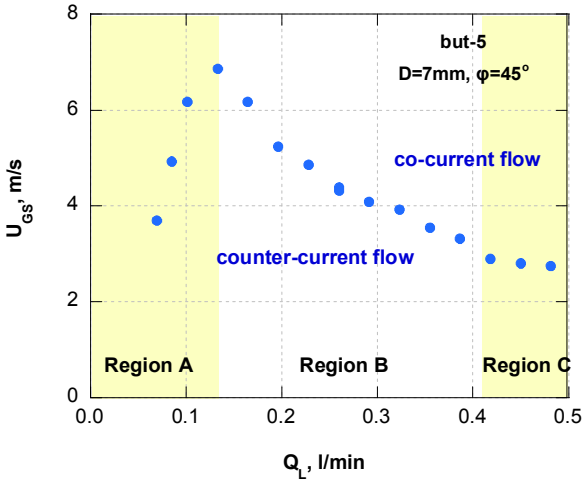

Figure 5: Typical flooding curve (*but-5*, φ=30°, D=7 mm).

The effect of tube diameter is depicted in ***Figure 6***. It is obvious that the flooding velocity increases with increasing diameter, a trend observed for all the liquids and inclination angles tested, and it is in accordance with available literature (e.g. Koizumi & Ueda, 1996; Mouza et al., 2002). Also the extent of *Region A* is reduced with tube diameter, i.e., it shrinks for the 9 mm tube i.d.

Flooding velocity tends to increase with inclination angle, as depicted in ***Figure 7*** for the 9 mm i.d. tube, where this trend is more pronounced. This is in accordance with the observations by Barnea et al. (1986) and Fiedler et al. (2002), who suggest that higher flooding velocities are observed for inclinations between 45° and 60°.

In ***Figure 8*** the effect of liquid properties, i.e., surface tension and viscosity is shown. As expected (e.g. Clift et al., 1966) flooding velocity decreases as the viscosity increases (water-glycerine solutions). It is also obvious that the effect of surface tension is not significant, although a slight decrease is observed when surface tension decreases (water-butanol solution). The Tween solution exhibit a peculiar behaviour (higher flooding velocity for lower surface tension liquid), which will be explained in a following section.

Visual observations

In the case of counter-current flow in inclined tubes a stratified pattern is observed (***Figure 9***). Fast video recordings

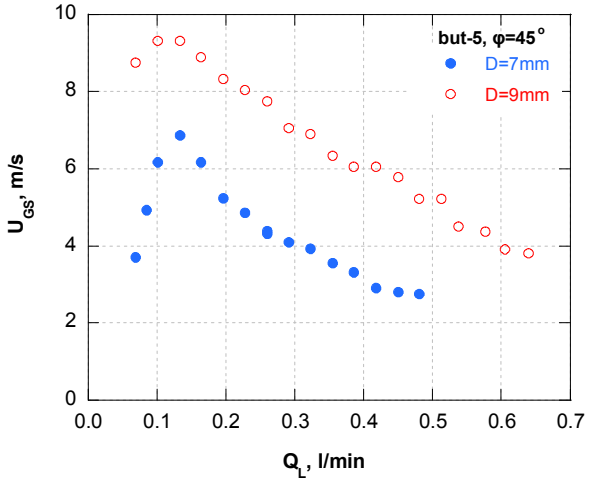

Figure 6: Effect of tube diameter on flooding velocity (*but-5*, φ=45°).

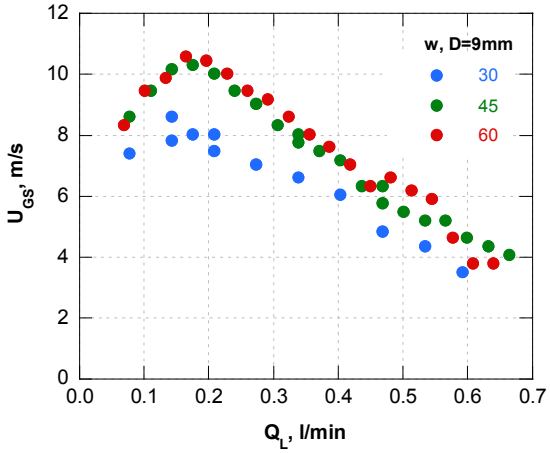

Figure 7: Effect of inclination angle on flooding velocity (*w*, D= 9 mm).

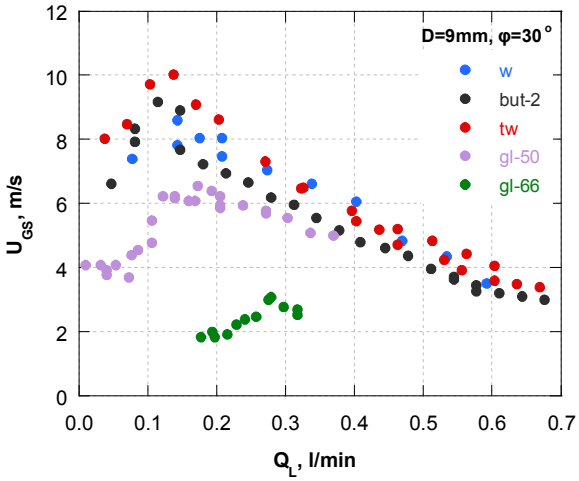

Figure 8: Effect of liquid properties on flooding velocity (D=9 mm, φ=30°).

reveal that at low gas flow rates the liquid surface appears smooth and undisturbed, but as the gas velocity increases small amplitude waves begin to form on the liquid surface. In ***Region A*** flooding is initiated near the liquid exit and the

flooding mechanism is wave levitation and upward transport. The liquid layer is decelerated at that point by the incoming air, resulting in a local lump, which is finally transported upwards (***Figure 10***).

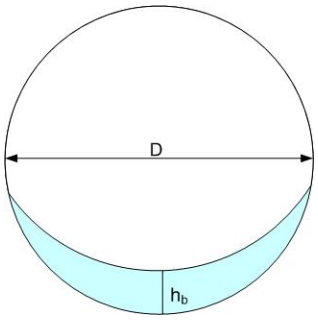

Figure 9: Schematic of the cross-section of the flow.

For the smaller diameter tube the waves appearing just before flooding initiation tend to spread in the circumferential direction, creating fairly coherent ‘‘ring’’-type waves, as shown in ***Figure 11***. For the larger diameter tube growth of standing waves at the liquid exit and reversal of their motion is again observed. The existence of *Region A* is more pronounced in the smaller diameter tubes, where the formation of ‘‘ring’’-type waves (through wave spreading) is apparently easier.

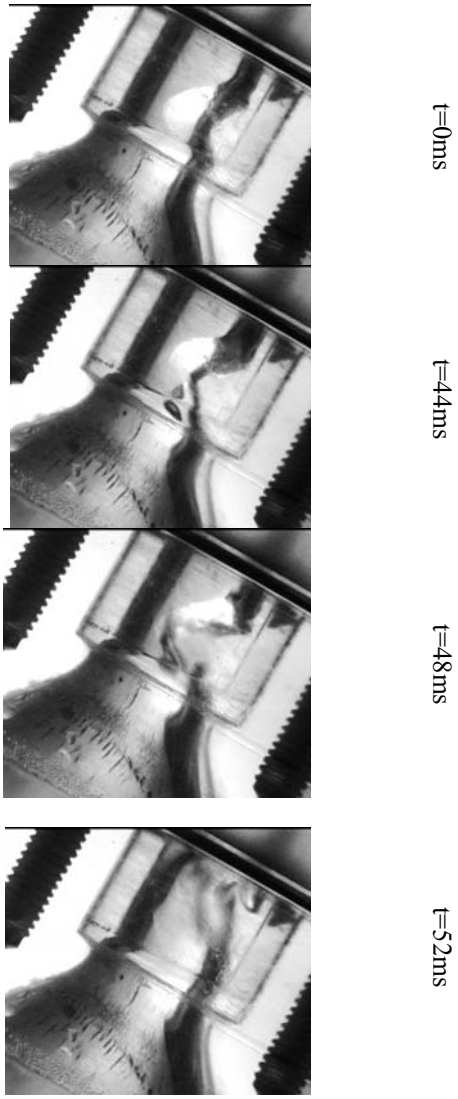

Figure 10: Exit flooding at *Region A* (*gl-30*, D=7 mm, φ=30°).

In ***Region B***, flooding is also initiated somewhere inside the tube by the growth and the upward transport of the waves formed on the liquid layer. At the onset of flooding, the waves reverse their flow direction, while spreading in the lateral direction and disintegrating to a limited extent into small droplets (***Figure 12***).

Finally, in ***Region C*** flooding is initiated at the liquid inlet, where a local disturbance tends to grow and block the tube. Consequently, this region is clearly observed at relatively high liquid flow rates.

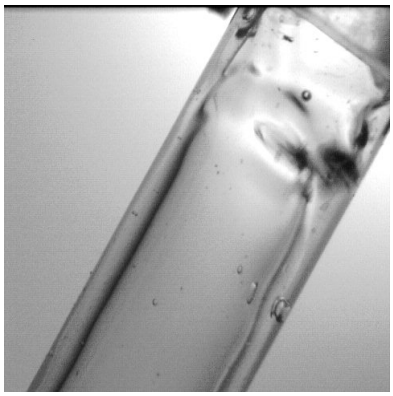

Figure 11: “Ring” type wave formed during flooding in *Region A* (*gl-30*, D=7 mm, φ=60°).

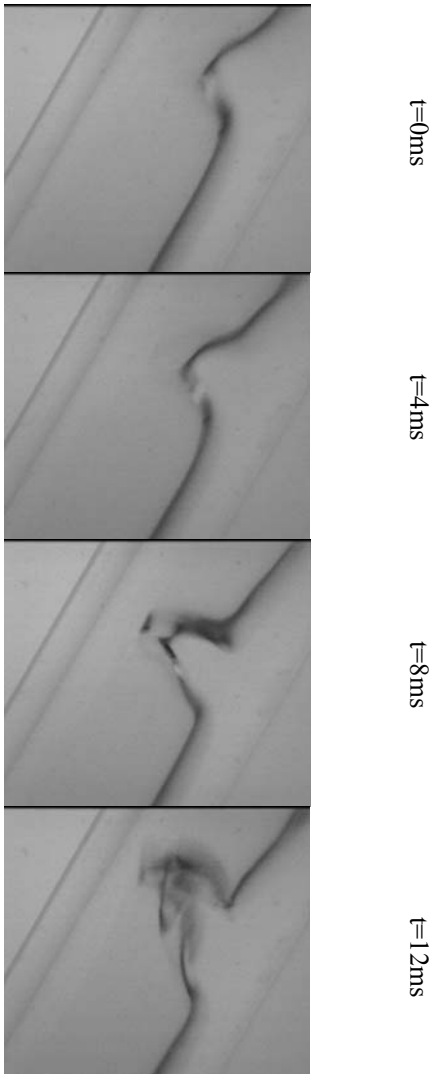

Figure 12: Exit flooding at *Region B* (*tw*, D=7 mm, φ=60°).

Free falling liquid layer

In order to better understand the influence of the ***liquid properties*** on the falling liquid layer development, free falling liquid layer, i.e., liquid flow without counter-current gas, has been studied. Thus, the characteristics of a free falling liquid layer were recorded using the high-speed camera near the liquid exit. As it was expected, the measurements reveal that the liquid layer becomes thicker as viscosity increases, while the effect of surface tension seems to be insignificant.

The obtained results are not in good agreement with the theoretically predicted liquid layer thickness values either by the correlation proposed by Mouza et al. (2003), which accounts for laminar flow in inclined tubes, or the correlation by Lioumbas et al. (2005), that takes into account also the transition from the laminar to turbulent flow. This deviation of the experimental data from the models could be attributed to the fact that the aforementioned correlations are based on the assumption that the shape of the interface is plane. Closer inspection of the flow pattern exhibits, however, that this is not the case for the flow in small diameter inclined tubes, where the capillary forces become quite significant. Photos of the cross section of the tube taken at the liquid exit indicate that the interface is concave for all the liquids, diameters and inclination angles tested (***Figure 13***).

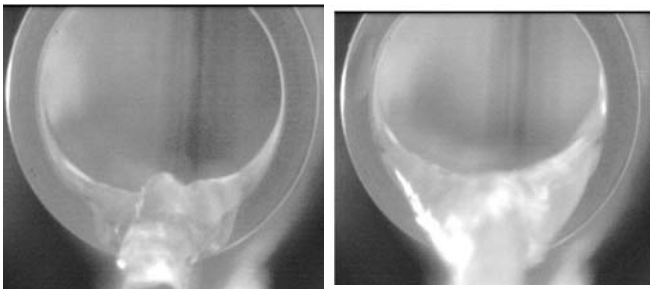

(a) (b)

Figure 13: Typical photos of the tube cross section at the liquid exit for water at a) Q_L=0.16 l/min and b) Q_L=0.64 l/min (φ=30°).

Measurements using the conductivity method are taken near the liquid exit. In ***Figure 14*** typical water free falling layer thickness normalized with respect to its mean value are presented. For low flow rates the liquid layer is smooth and undisturbed (***Figure 14a)***. As liquid flow rate increases, solitary waves appear (***Figure 14b)***, whose frequency increases with flow rate. For even higher flow rates the waves become more frequent, tending to merge with each other, resulting in an increased liquid layer thickness with more frequent fluctuations (***Figure 14c)***. Lioumbas et al. (2005), who studied co-current gas-liquid stratified flow in 24 mm i.d. slightly inclined tube, observed similar wave patterns and suggest that the appearance of solitary waves is associated with the transition from laminar to turbulent flow.

The root mean square values of the layer thickness fluctuations extracted from the statistical analysis of the layer thickness time series, which can serve as a measure of the wave height, are presented in ***Figure 15*** versus Q_L for water in the 9 mm i.d. tube and for various inclination angles. The liquid layer is practically undisturbed up to a critical flow rate after which the solitary waves make their appearance and the wave amplitude begins to increase. After a certain Q_L the waves merge and the wave amplitude decreases, as it was also shown in ***Figure 14c***.

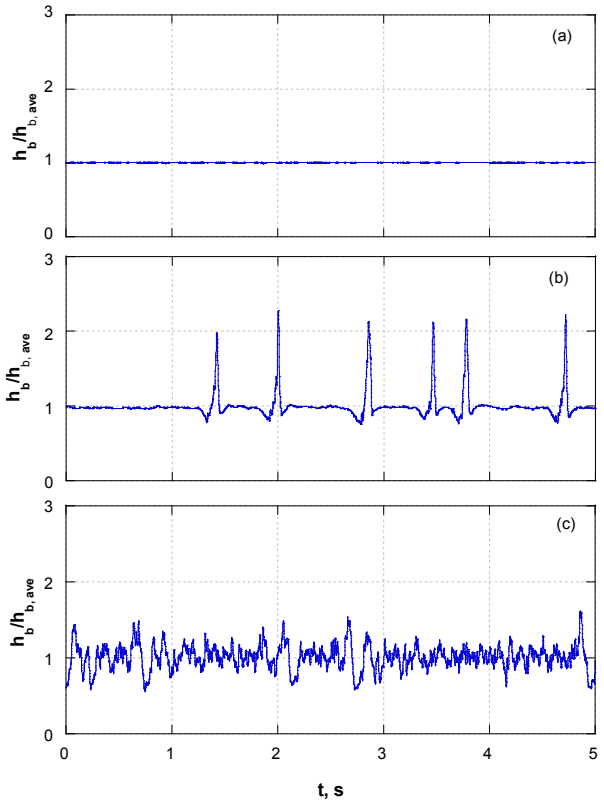

Figure 14: Typical water free falling layer thickness normalized with respect to the mean value for a) Q_L=0.25 l/min, b) Q_L=0.49 l/min and c) Q_L=0.73 l/min (D=9 mm, φ=45°).

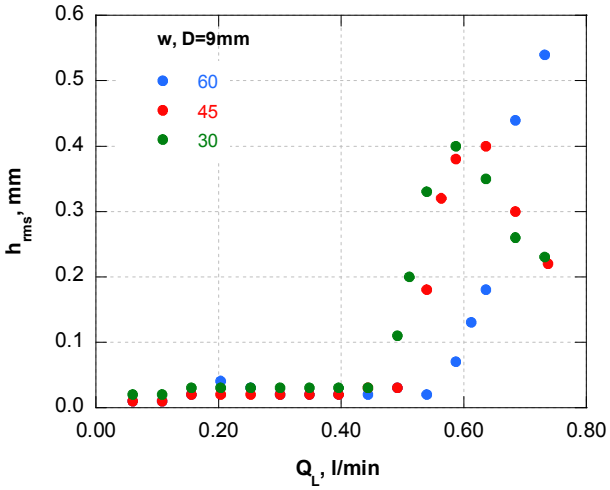

Figure 15: Typical h_{rms} versus Q_L for various inclination angles (w, D=9 mm).

Figure 16 presents simultaneous recordings of the wall shear stress and the liquid layer thickness variation versus time collected in two measuring points, which are about 6 cm apart**.** As it is expected, the two signals are very well related to each other, a fact that is also depicted in the cross correlation function of ***Figure 17***.

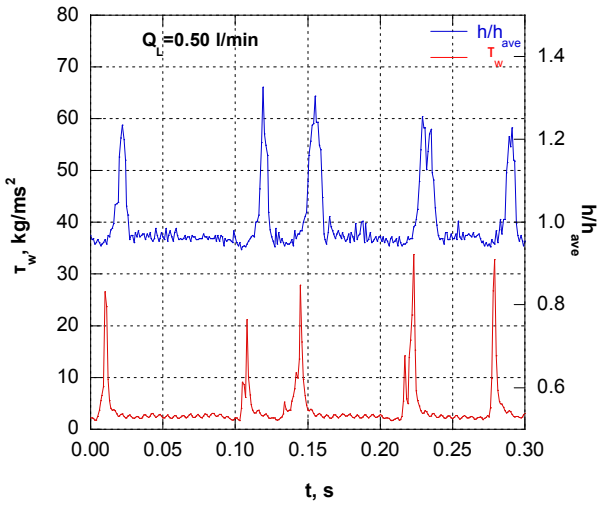

Figure 16: Typical wall shear stress trace and liquid layer thickness fluctuations for free falling liquid layer (Q_L=0.50 l/min, D=9 mm, φ=30°).

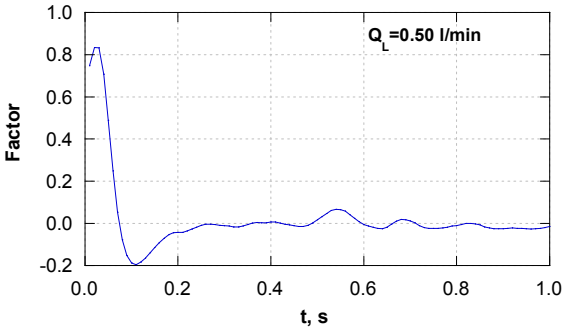

Figure 17: Cross correlation of the shear stress and liquid layer thickness time series (Q_L=0.50 l/min, D=9 mm, φ=30°).

Incipient flooding and mechanisms

The wall shear stress measurements, which can serve as an indication of the interfacial condition, are used in an effort to interpret the mechanisms prevailing during flooding. As it is already mentioned, in *Region A* gas flooding velocity increases with liquid flow rate. This trend has been reported only for small diameter tubes and its existence may be attributed to big curvature, since the phenomenon also seems to diminish as the diameter increases. It is suggested that the big tube curvature (i.e., small i.d. tube) promotes lateral liquid spreading, thus reducing the possibility of wave formation (Mouza et al., 2003). This is also depicted in ***Figure 18*** and ***Figure 19***, where even just before flooding onset, very small interfacial fluctuations exist. In this case, the incoming air decelerates the liquid layer and as a result a lump is created because of the accumulation of the liquid. Finally, the increased drag force exerted by the air leads to flow reversal. As liquid flow rate increases, the momentum of the liquid layer increases and consequently the force needed to "freeze" the liquid layer and reverse its flow also increases.

In ***Figure 20*** typical wall shear stress time series for three pairs of liquid flow rates and gas velocities a little lower than the necessary to cause flooding, are presented. At Q_L=0.06 l/min, which corresponds to *Region A*, the disturbances of the wall shear stress and consequently of the layer thickness are low, with small waves of longer amplitude

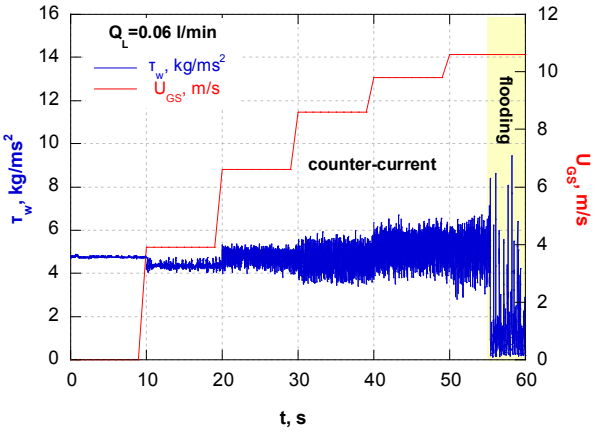

Figure 18: Wall shear rate and gas flow rate change during counter-current air-*fer* flow (Q_L=0.06 l/min, D=9 mm, φ=45°).

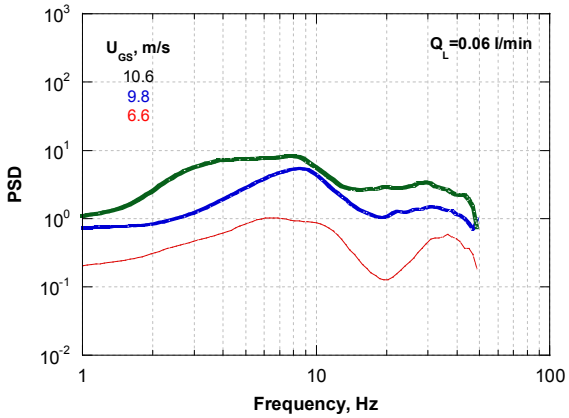

Figure 19: Power spectral density of wall shear stress fluctuations at various U_{GS} before flooding onset (Q_L=0.06 l/min, D=9 mm, φ=45°).

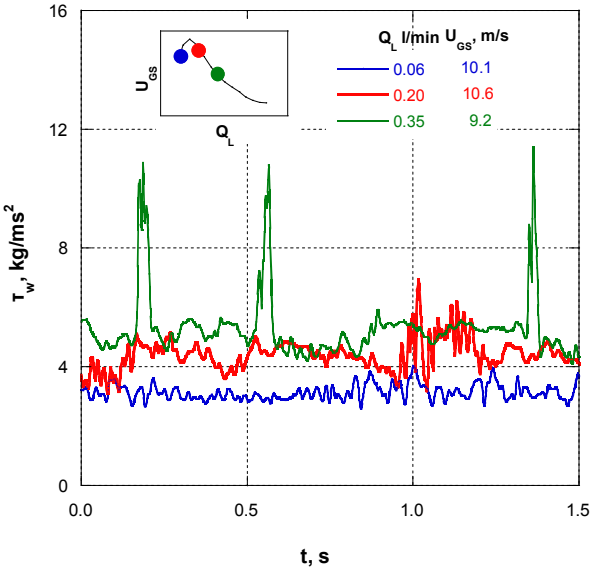

Figure 20: Wall shear stress recordings for various liquid flow rates just before incipient flooding.

being formed on the interface. For liquid flow rate close to the transition from *Region A* to *B* the fluctuations become more intense and higher waves appear. The emergence of

these waves facilitates flooding initiation. Further increase of the liquid flow rate (Q_L=0.35 l/min, *Region B*) results in larger waves being formed and consequently as these waves grow larger with liquid flow rate, flooding velocities are reduced (*Region B*).

In ***Figure 21*** the wall shear stress during gas-liquid counter-current flow along with the gas superficial velocity are plotted for a liquid flow rate that corresponds to *Region B*. For the free falling liquid layer, i.e., U_{GS}=0, wall shear stress is smooth and undisturbed. For the lower gas flow rates, the wall shear stress remains smooth but a small reduction of its value is observed. For higher gas superficial velocity disturbances are recorded, which become more intense as gas flow rate further increases. Just before incipient flooding large waves appear and flooding is initiated. At this point the wall shear stress decreases rapidly. Total reversal of the flow, however, is not observed. The wall shear stress measurements show no evidence of liquid film flow reversal up to the onset of flooding; in fact they indicate that part of the liquid is still flowing downwards even after flooding initiation.

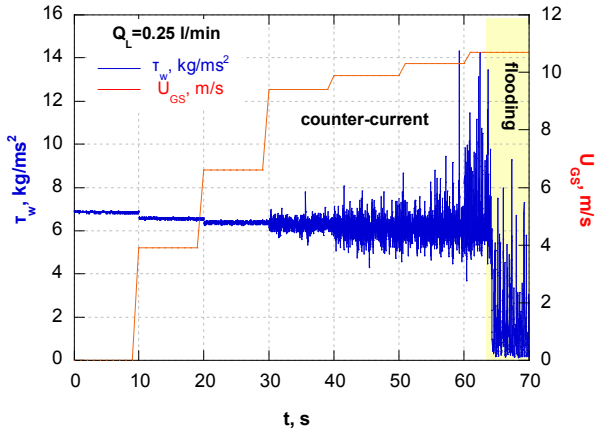

Figure 21: Wall shear stress and gas flow rate change during counter-current air-*fer* flow (Q_L=0.25 l/min, D=9 mm, φ=45°).

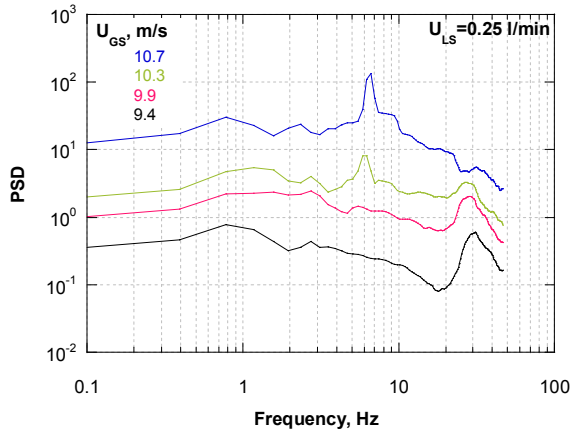

Figure 22: Power spectral density of wall shear stress fluctuations at various U_{GS} before flooding onset (Q_L=0.25 l/min, D=9 mm, φ=45°).

Spectral analysis of the signal reveals that disturbances occurring as gas flow rate increases are at first about 30 Hz and only some small fluctuations can be observed with a frequency of less than 1 Hz (***Figure 22***). As gas velocity increases waves appear at a frequency around 5-6 Hz. With a further small increase in gas flow rate and just before the onset of flooding these waves grow rapidly and lead to flow reversal and flooding in the tube.

The previous observations confirm that flooding initiation depends on the waves formed on the gas-liquid interface. According to this, the effect of liquid properties on flooding can be clarified. As reported in the literature, viscous liquids exhibit thick liquid layers, and large amplitude waves grow even for very low flow rates (e.g. Mouza et al., 2005; Nguyen & Balakotaiah, 2000). This fact facilitates flooding initiation and thus lower flooding velocities are observed in this case (***Figure 8***). Increasing surface tension values seem to invoke a stabilizing effect on the interface, while lower values lead to rougher interface (Lioumbas et al., 2006). Its effect though is not very significant, thus flooding is not greatly influenced, as already mentioned. However, in the case of surfactant solutions, (e.g. Tween solution) a considerable damping of the roll-wave amplitude is observed, despite the fact that the reduced liquid surface tension in gas–liquid stratified flows generally causes higher interfacial waves (Lioumbas et al., 2006). For this reason flooding is achieved for higher gas velocity, regardless of its lower surface tension (***Figure 8***).

Existing correlations could obviously not predict flooding velocity in *Region A*, since these data do not follow the common trends reported in the literature. In *Region B* flooding velocities are roughly correlated by a Wallis-type equation. The correlation proposed by Mouza et al. (2003), which refers also to data from *Region B* but assumes a plane surface of the liquid layer, as expected shows a rather poor agreement with the present experimental data. An attempt will be made, and indeed is currently in progress, to modify the aforementioned correlation so as to take into account the effect of the concave surface.

Conclusions

Flooding velocities were measured for various liquids, three inclination angles, i.e 30°, 45° and 60°, and two tube diameters. At the lower liquid flow rates employed the critical gas velocity for incipient flooding tends to increase almost linearly with Q_L (*Region A*). This seems to be due to lateral spreading of liquid (near the exit) facilitated by the large tube curvature. At intermediate Q_L (*Region B*) the flooding velocity tends to decrease with increasing liquid flow rate, as observed with relatively large i.d. tubes in the literature. The growth of 3-D waves along the tube and reversal of their flow direction is the mechanism for incipient flooding in this region. At even higher liquid flow rates (*Region C*) the flooding velocity tends to be independent of liquid flow rate, a fact that is attributed to the growth of disturbances at liquid inlet leading to an instantaneous flow reversal.

Flooding is facilitated as viscosity increases. The effect of surface tension on flooding onset is not very important. However, in the case of surfactant solutions flooding initiation is delayed, despite their reduced surface tension, due to considerable damping of the roll-wave amplitude.

The free-flowing liquid layer data reveal a smooth surface with long wavelength waves appearing only at the higher liquid flow rates investigated. The emergence of these waves is promoted by the counter-current gas flow. In general, the liquid layer characteristics show that significant changes occur in liquid film flow only under conditions approaching flooding.

The wall shear stress fluctuations (measured at the bottom centerline of the tube) are in accordance with layer thickness fluctuations, for free flowing liquid layers. Therefore, the electrodiffusion method turns out to be a useful non-intrusive tool for monitoring the instantaneous changes of the film thickness in the case of very thin liquid layers.
The liquid layer surface was found to be concave and not plane for the geometries studied, and therefore the layer thickness could not be successfully predicted by existing correlations.
Data processing and interpretation is currently in progress in an effort to elucidate the effects of liquid properties on flooding. Furthermore, dimensionless numbers will be employed in generalized correlations for predicting the transition between consecutive flooding regions, which would be applicable in equipment design.

Acknowledgements

Financial support by the General Secretariat for Research & Technology and the European Union (PENED 2003) is greatly acknowledged.
Dr Vaclav Sobolik and Dr Jaroslav Tihon are greatly acknowledged for the preparation of the electrodiffusion probes and their contribution to this work. The authors would also like to thank Mr. A. Lekkas, Mr. T. Tsilipiras and Mr. F. Lambropoulos for the technical support.

References

Alekseenko, S.V., Nakoryakov, V.E., Pokusaev, B.G. (1994) Wave flow of liquid films. Beggel House, Inc., NY.

Bankoff, S. G. & Lee, S. C. (1986). "A critical review of the flooding literature." Hewitt, G.F., Delhaye, J.M., Zuber, N. (Eds.), Multiphase Science and Technology., Hemisphere Corp, NY.

Barnea, D., Ben Joseph, N. & Taitel, Y. Flooding in inclined pipes- Effect of entrance section. Canadian J. Chem. Eng., 64, 177-184 (1986).

Celata, G. P., Cumo, M. & Setaro, T. Flooding in inclined pipes with obstructions. Exp. Thermal Fluid Science, 5, 18-25 (1992).

Cetinbudaklar, A. G. & Jameson, G. J. The mechanism of flooding in vertical countercurrent two-phase flow. Chem. Eng. Sci., 24, 1669-1680 (1969).

Clift, R., Pritchard, C. L. & Nederman, R. M. The effect of viscosity on the flooding conditions in wetted wall columns. Chem. Eng. Sci., 21, 87-95 (1966).

Dukler, A. E., Smith, L. & Chopra, A. Flooding and upward film flow in tubes—I. Int. J. Multiphase Flow, 10, 585-597 (1984).

English, N. J. & Kandlikar, S. G. An experimental investigation into the effect of surfactants on air-water two-phase flow in minichannels. Heat Transfer Engineering, 27(4), 99-109 (2006).

Fiedler, S., Auracher, H. & Winkelmann, D. Effect of inclination on flooding and heat transfer during reflux condensation in a small diameter tube. Int. Comm. Heat Mass Transfer, 29, 289-302 (2002).

Hewitt, G. F. "In search of two-phase flow, lecture." 30th US National Heat Transfer Conference, Portland, Oregon (1995).

Jayanti, S., Tokarz, A. & Hewitt, G. F. Theoretical investigation of the diameter effect on flooding in counter-current flow. Int. J. Multiphase Flow, 22, 307-324 (1996).

Koizumi, Y. & Ueda, T. Initiation conditions of liquid ascent of the counter-current two phase flow in vertical pipes (in the presence of two-phase mixture in the lower portion). Int. J. Multiphase Flow, 22, 31-43 (1996).

Lioumbas, J. S., Paras, S. V. & Karabelas, A. J. Co-current stratified gas-liquid downflow--Influence of the liquid flow field on interfacial structure. Int. J. Multiphase Flow, 31(8), 869-896 (2005).

Lioumbas, J. S., Mouza, A.A. & Paras, S. V. Effect of surfactant additives on co-current gas–liquid downflow. Chem. Eng. J., 61, 4605-4616 (2006).

Mitchell, J.E. Hanratty, T.J. A study of turbulence at a wall using an electrochemical wall-shear-stress meter. J. Fluid. Mech., 26, 199-221 (1966).

Mouza, A. A., Pantzali, M. N. & Paras, S. V. Falling film and flooding phenomena in small diameter vertical tubes: The influence of liquid properties. Chem. Eng. Sci., 60(18), 4981-4991 (2005).

Mouza, A. A., Paras, S. V. & Karabelas, A. J. The influence of small tube diameter on falling film and flooding phenomena. Int. J. Multiphase Flow, 28, 1311-1331 (2002).

Mouza, A. A., Paras, S. V. & Karabelas, A. J. Incipient flooding in inclined tubes of small diameter. Int. J. Multiphase Flow, 29(9), 1395-1412 (2003).

Nguyen, L. T. & Balakotaiah, V. Modelling and experimental studies of wave evolution on free falling viscous films. Phys. Fluids, 12, 2236-2256 (2000).

Ousaka, A., Deendarlianto, Kariyasaki, A. & Fukano, T. Prediction of flooding gas velocity in gas-liquid counter-current two-phase flow in inclined pipes. Nucl. Eng. Des., 236(12), 1282-1292 (2006).

Paras, S. V. & Karabelas, A. J. Properties of the liquid layer in horizontal annular flow. Int. J. Multiphase Flow, 17(4), 439-454 (1991).

Shearer, C. J. & Davidson, J. F. The investigation of a standing wave due to gas blowing upwards over a liquid film; its relation to flooding in wetted-wall columns. J. Fluid Mech., 22, 321-335 (1965).

Suzuki, S. & Ueda, T. Behaviour of liquid films and flooding in counter-current two-phase flow-Part 1. Flow in circular tubes. Int. J. Multiphase Flow, 3, 517-532 (1977).

Tihon, J., Tovchigrechko, V., Sobolik, V. & Wein, O. Electrodiffusion detection of the near-wall flow reversal in liquid films at the regime of solitary waves. J. Appl. Electrochem., 33, 577-587 (2003).

Wallis, G. B. (1969) One-dimensional Two-phase Flow. McGraw-Hill, NY.

Wongwises, S. Effect of inclination angles and upper end conditions on the countercurrent flow limitation in straight circular pipes. Int. Commun. Heat Mass Transfer, 25,

117-125 (1998).

Zabaras, G. J. & Dukler, A. E. Countercurrent gas–liquid annular flow, including the flooding state. AIChE J., 34, 389-396 (1988).

Zapke, A. & Kroeger, D. G. The influence of fluid properties and inlet geometry on flooding in vertical and inclined tubes. Int. J. Multiphase Flow, 22, 461-472 (1996).

Zapke, A. & Kroeger, D. G. Countercurrent gas-liquid flow in inclined and vertical ducts - I: Flow patterns, pressure drop characteristics and flooding. Int. J. Multiphase Flow, 26, 1439-1455 (2000a).

Zapke, A. & Kroeger, D. G. Countercurrent gas-liquid flow in inclined and vertical ducts - II: The validity of the Froude-Ohnesorge number correlation for flooding. Int. J. Multiphase Flow, 26, 1457-1468 (2000b).